Ingénierie des Systèmes d'Information
Vol. 31, No. 3, March, 2026, pp. 819-834
Journal homepage: http://iieta.org/journals/isi

Aquilla Optimization Based K-Means Clustering for Brain Tumor Segmentation with Outlier Detection

Pooja Singh[1*], Sunanda Sharda[1], Sanoj Kumar[2]

[1] Department of Physics, School of Basic and Applied Sciences, SGT University, Gurugram 122505, India
[2] Data Science Cluster, SOCS, UPES, Dehradun 248007, India

Corresponding Author Email: pujasingh0409@gmail.com

https://doi.org/10.18280/isi.310315

Received: 3 October 2025
Revised: 10 December 2025
Accepted: 16 December 2025
Available online: 31 March 2026

Keywords:
magnetic resonance imaging, Aquila optimization, K-means clustering, brain tumor segmentation, adaptive histogram equalization

ABSTRACT

Brain tumors are one of the leading causes of worldwide health challenges. Due to the complexity of their location, shape, and size, as well as the lengthy diagnostic process, detecting tumors early can be quite challenging. Existing systems need to handle a variety of issues, including diverse image content, cluttered objects, occlusion, image noise and non-uniform object textures. To overcome these issues, a clustering-based segmentation with effective pre-processing approach is developed for accurate segment of tumor region. Clustering algorithms automatically group similar data points (pixels, in the case of images) into clusters, discovering inherent patterns in the data without any prior knowledge and are computationally less expensive. They possess ability to handle heterogeneous data and robustness to noise by detecting outlier. Initially, a median filter and a Wiener filter are applied to reduce noise. After noise reduction, adaptive histogram equalization (AHE) is used to improve the contrast of brain tumor images. Following that, Gamma correction is applied during preprocessing to adjust the overall brightness of the brain tumor image. The optimal K-means clustering algorithm for tumor segmentation uses *K* centroids to divide the data into *K* clusters. By employing the Aquila optimization algorithm, the centroid selection process is enhanced, effectively distinguishing the tumor region from the background. This improvement overcomes limitations and results and leads to better segmentation performance. The proposed system achieved a Peak Signal-to-Noise Ratio (PSNR) of 60.14 dB, a Bit Error Rate (BER) of 0.016, a Structural Similarity Index Measure (SSIM) of 0.99, and a Normalized Correlation (NC) of 0.60, all of which are better than the current system.

1. INTRODUCTION

A brain tumor is an aberrant, neoplastic growth of brain tissue. The two main kinds of brain tumors, sometimes referred to as lesions or neoplasia, are primary and metastatic tumors [1]. Primary brain cancers originate in the brain and its surrounding tissues. Brain tumors frequently have fatal effects due to its dangerous effects thus it is considered as a serious illness [2]. Hence, the study of brain tumor images has recently received increasing attention. Nowadays, a variety of modalities are employed to obtain various types of medical images, including positron emission tomography, magnetic resonance imaging (MRI), computed tomography (CT), and X-rays [3]. Among these distinct modalities MRI is suitable for brain imaging, because it can be done without providing radioisotopes [4]. MRI comprises a vast quantity of information and which is a multi-parameter-based imaging that can create diverse images through altering various parameters [5]. However, noise in MRI images sometimes results in low contrast, which makes it difficult to accurately identify lesion locations.

Tumor segmentation is effective and therefore crucial. A range of image segmentation methods are currently often used in medical image segmentation [6]. Because, in decision-oriented applications, image segmentation is an important and thorough way to accurately identify an image's pixel values. Several segmentation techniques, including edge-based, threshold-based, and neural network-based methods, are commonly employed in medical applications to aid in the diagnosis of various diseases [7]. However, these segmentation methods often yield suboptimal results, especially when applied to imaging of brain tumors. Segmentation based on threshold estimates the threshold based on particular properties of each pixel. Next, the pixel feature values are compared to the segmentation threshold in order to identify which regions of the features [8]. Using certain pixel boundary directions, edge-based segmentation establishes the boundaries [9]. One of the trickier parts of neural networks in neural network-based segmentation is creating the network [10]. The creation of neural networks is challenging since it takes a lot of time and calculation.

Techniques for clustering images are widely used in medical picture segmentation. Expectation maximization (EM), K-means clustering, fuzzy C-means clustering (FCM), and K-means++ clustering [11]. Fuzzy set theory makes soft segmentation possible, which is the foundation for how FCM-

based segmentation operates. Data can be described as a collection of probability distributions in accordance with the EM technique [12]. The program then repeatedly computes the posterior probability and estimates the mean, covariance, and mixture coefficients by applying the maximum likelihood estimation method along with clustering criteria [13]. The majority of these clustering techniques are susceptible to noise [14]. The K-means clustering method presents several challenges, as it calculates the distances between the image's pixels and the cluster centroids. It then assigns each pixel to the class corresponding to the nearest centroid, updating the grayscale means of the clusters through iterative steps [15]. To address this concerns in this research proposed an Aquila optimization-based K-means clustering for selecting optimal cluster centroids. Consequently, an effective clustering segmentation method was presented in this research to improve unstable clustering and lessen noise sensitivity. The research work's primary contribution is listed below:

- An effective brain tumor segmentation model is presented utilizing an Aquila optimization-based K-means clustering algorithm.
- Preprocessing techniques are used to enhance the quality of the brain tumor image. Noise is removed from the brain image using both the median filter and the Wiener filter.
- An adaptive histogram equalization (AHE) technique, along with gamma correction, is applied to improve the contrast of the brain MRI pixels.
- Using the optimal K-means clustering algorithm for tumor segmentation which work based on the K-centroids, it divides or clusters the provided data into K-clusters or portions.
- In K-means clustering, the centroid is strategically selected to efficiently segment the region of interest from the background. The centroids of each cluster are determined using the Aquila optimization algorithm (AOA).

The structure of the remaining sections of the research is outlined as follows: Section 2 reviews several studies related to the current methodology. Section 3 provides a brief overview of the proposed brain tumor segmentation process. Section 4 presents the results and performance evaluation of the proposed framework. Finally, Section 5 concludes the study.

2. RELATED WORK

A number of clustering methods have recently been presented by different researchers to help segment tumors in brain scans and assess the disease's state. Thus, the methods that are most frequently employed for segmentation are K-means, K++, and FCM. Several techniques are reviewed here, some of which come from these techniques.

Karun et al. [16] introduced a hybrid method combining Elephant Herding Optimization (EHO) and Entropy-Driven Fuzzy C-Means (EnFCM) clustering to improve brain tumor segmentation accuracy. EHO optimizes the clustering process, enhancing tumor boundary detection, while EnFCM accounts for intensity inhomogeneity. Evaluated on the Brain Tumor Segmentation (BraTS) dataset, the method outperforms traditional approaches across key metrics such as dice similarity, mean-square error (MSE), Peak Signal-to-Noise Ratio (PSNR), and Tanimoto coefficient.

Islam et al. [17] introduced a more efficient way of detecting brain cancers in humans that uses principal component analysis (PCA) and superpixels in conjunction with the template-based K-means (TK) method. Initially, this technique used both PCA and superpixels to extract important features that aid in the precise diagnosis of brain tumors. Next, accuracy is increased by enhancing the image with a filter. Lastly, image segmentation is performed using the TK-means clustering technique to locate the brain tumor.

Sharif et al. [18] presented a brain tumor segmentation and classification method using improved saliency segmentation and feature selection. The method follows four steps such as tumor preprocessing (Region of Interest extraction and noise removal with a Gaussian filter), tumor segmentation via an enhanced thresholding technique, feature extraction (geometric and texture features), and classification using a support vector machine (SVM) with a linear kernel. Features are selected using a genetic algorithm (GA) for optimal accuracy.

Sahoo et.al [19] presented a hybrid deep convolutional neural network (CNN) model, combining a pretrained ResNet101 with 12 additional layers. The method operates in three stages in first, the hybrid CNN was trained on BraTS 2020 and BraTS 2017 multi-parametric MRI (mPMRI) datasets to detect the whole tumor. Second, the tumor core and edema regions are segmented using the Local Center of Mass (LCM) method. Finally, K-means clustering extracts the tumor core and edema.

Kumar et al. [20] presented an automatic MRI brain tumor classification system for efficient brain tumor image categorization and grading. The four components that make up the suggested task are classification, segmentation, feature extraction, and pre-processing. Since noise in the input images could affect the accuracy of the classification process, it was first removed using a median filter. The photos are instantly transformed into 3 × 3 blocks. Next, the pre-processed image's texture features are extracted. The adaptive k-nearest neighbor classifier uses the features obtained from the feature extraction procedure to determine whether an image is normal or abnormal. Afterwards, the best probabilistic fuzzy C-means clustering algorithm is used to segment the tumor regions.

According to the reviewed articles, the brain tumor segmentation process has more complexity for attaining better findings. Therefore, it is essential to find tumors early in order to save and extend the patient's life. As a result, improved brain tumor identification is necessary in the medical industry. However, the currently available methods such as, random forest, artificial neural network (ANN), wavelet transform, fuzzy c-means, etc. can only diagnose brain cancers with insufficient accuracy and a lengthy execution time [17], Segmentation model was sensitive to choose parameter [16]. MRI diagnosis may be flawed, due to the distortions and noise present in the segmentation technique [18]. This can cause normal tissue to be mistaken for abnormal tissue. In addition, as tumors spread at different speeds from their surroundings, it is also necessary to simulate their ontogenesis [19]. As a result, segmenting magnetic resonance (MR) brain pictures remains difficult due to potential noise, bias fields, and partial volume effects [20]. The proposed model addresses these issues by utilizing K-means clustering, a computationally efficient and simple method, enhanced with the AOA. This optimization improves the selection of centroids, overcoming K-means' typical limitations and providing more accurate and reliable tumor segmentation. The combination of K-means

clustering with Aquila optimization allows for better handling of noise, distortion, and tumor heterogeneity, offering a promising solution for faster, more accurate, and clinically feasible brain tumor detection.

3. PROPOSED METHODOLOGY OF BRAIN TUMOR SEGMENTATION

Aquila optimization-based K-means clustering for brain tumor segmentation is presented in this work. Image segmentation is considered as a significant process for properly identifying the pixel values of an image during classification. Generally, for segmentation, medical images are gathered from distinct modalities like X-ray, positron emission tomography CT, and MRI. Among these distinct modalities MRI is suitable for identifying the abnormal alternations in organs as well as tissues in the brain through segmentation. Thus, using clustering-based techniques that separate a range of similar sorts of components or colors into many clusters using gray and color intensity similarities, the tumors present in the MRI are segmented. Nevertheless, the majority of earlier clustering techniques are noise content sensitive. As a result, this study suggests an effective clustering segmentation technique to improve unstable clustering and lessen noise sensitivity. Figure 1 shows the architecture of the suggested brain tumor segmentation model.

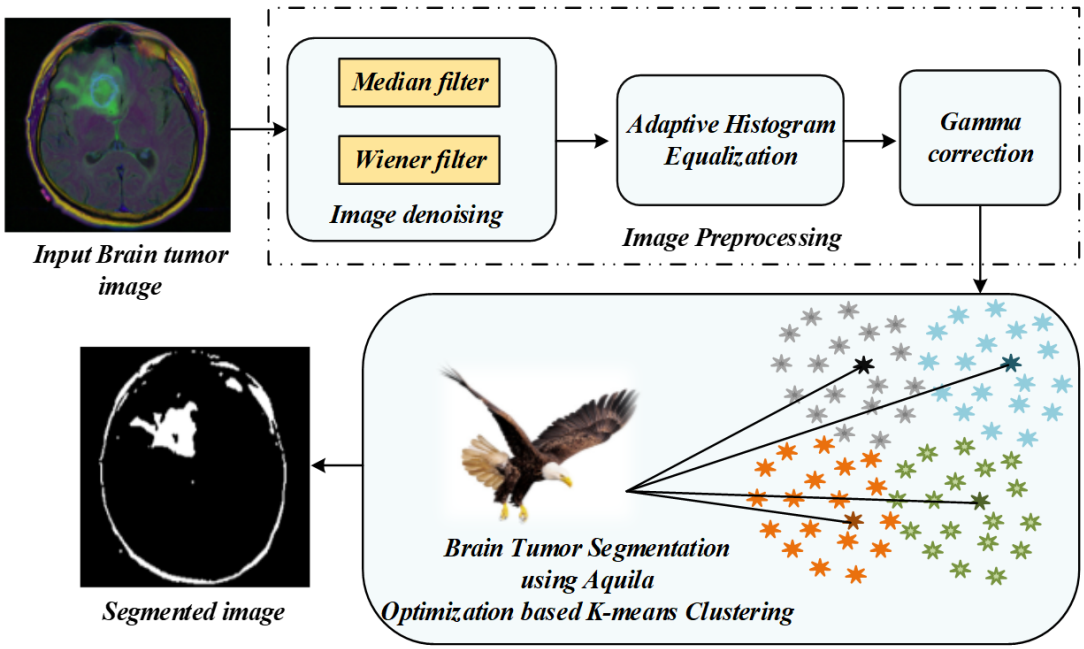

Figure 1. Architecture of the proposed brain tumor segmentation model

There are two stages in the suggested brain tumor segmentation model: image preprocessing and tumor segmentation. The first step is image preprocessing, which is done to improve the characteristics and quality of the image in order to obtain reliable results. In the preprocessing stage, gamma correction, AHE, and image denoising are used. For envision denoising, the wiener and median filters are employed. For the elimination of noise and normalization of color median is used. A Wiener filter is employed to control the additive noise and blurring. An AHE is used after noise reduction to improve the contrast of the images of brain tumors. Finally, in the preprocessing phase applied a gamma correction to control the entire brightness of the brain tumor image. Once completed preprocessing, the preprocessed brain tumor image is given as the input of the segmentation phase. Here, segmentation is performed with the aid of improved K-means clustering for effective segmentation. The K-means clustering is improved using an AOA which can select the optimal cluster centroids effectively this can remove the burdens of conventional K-means clustering algorithm and perform segmentation effectively. The segmented tumor regions are then used as input into the CNN model which is trained to classify the image into brain diseases categories to validate the proposed segmentation model. The process comprises in the proposed model is described as follows.

3.1 Image preprocessing

The primary goal of image preprocessing is to simplify complex calculations, leading to improved results. These preprocessing techniques are designed to enhance image quality while preserving its original features. The following outlines the various preprocessing strategies applied in this method.

3.1.1 Image de-noising

The image de-noising process effectively reduces the noise present in brain tumor images. The different intrinsic or extrinsic circumstances that lead to the noise in the images can be challenging to deal with further process. Therefore, the median filter and wiener filter are the two different de-noising techniques considered in this method.

i) Median Filter

It is a type of nonlinear filter which is used to reduce noise like "pepper" as well as "salt" noise i.e., impulse noise that exists in the image. These filters move through the various parts of the image in terms of pixels by pixels. Instead of average the grey levels in a pixel, the median filter replaces the grey level of each pixel with the median of the grey levels in its immediate vicinity. The following expression shows the

median filter. The median filter is shown in the following expression:

$$f(x,y) = \underset{(s,t)\in S_{xy}}{\text{median}}\{g(s,t)\} \quad (1)$$

The median is calculated based on the initial value of the pixels. Median filters are widely used for specific types of random noise because they effectively reduce noise while causing much less blurring compared to linear smoothing filters of similar size.

ii) Wiener Filter

Wiener filters are widely used in image processing for restoration tasks, such as eliminating motion blur and optimizing image clarity. If a certain filter causes images to become blurry, inverse filtering can recover the original image. This technique lessens image degradation and enables the creation of restoration algorithms for each kind of degradation technique. Inverse filtering and noise smoothing are traded off in the Wiener filtering. When a color image is supplied to the wiener filter as an input. The channel with the greatest trade-off is used as the input image. Each channel's contrast was determined for the color channel selection. By utilizing a low pass filter, a wiener filter can measure the R, G, and B channels. It can be measured the contrast among the original images and the low pass filter image. The median and Wiener filters were selected for noise reduction, and the filter sizes were chosen to effectively handle impulse noise while minimizing blurring.

3.1.2 Adaptive histogram equalization

AHE is a technique similar to histogram equalization, but it further improves the contrast of input images by adjusting the enhancement process to local variations. The unique feature of AHE is its generation of multiple histograms, each of which represents a distinct part of the image. These histograms are then used to redistribute the brightness values, so strengthening the edges of each area of the image. Due to the extreme concentration of the histogram in fixed regions of the image, AHE may overestimate the contrast feature in the image. Utilizing AHE, it is possible to prevent the noise in neighbor-constant areas from being amplified. AHE can limit contrast amplification, hence which can resolve the issue of noise amplification. The AHE algorithm, which is based on probability theory recognizes the grey mapping of pixels present in the images by performing grey operations and which transforms the histogram to one that is uniformly smooth and has distinct grey levels in order to accomplish the goal of image enhancement.

Assume that the pixel in the original denoised brain tumor image has the grey value is denoted as $r(0 \le r \le 1)$ and $p(r)$ specifies the probability of its density. The pixel in the enhanced image has the grey value is specified as $s(0 \le s \le 1)$, $p(s)$ signifies the probability of its density and $s = T(r)$ represents the mapping function. Every point on the equalized histogram is of the same height, which is evident from the histogram's physics interpretation:

$$p_s(s)ds = p_r(r)dr \quad (2)$$

Assuming that the interval of the monotonically growing function is considered as $s = T(r)$ and its monotonically increasing inverse function is taken as $r = T^{-1}(s)$. According to Eq. (2), written the following Eq. (3) for both these functions:

$$p_s(s) = \left[p_r(r)\frac{1}{ds/dr}\right]_{r=T^{-1}(s)} = p_r(r)\frac{1}{p_r(r)} = 1 \quad (3)$$

The mapping relationship of i, which indicates that a pixel in the original image has a grey value, and f_i, which shows that a pixel in the enhanced image has a grey value, is the next discrete condition. Eq. (4) gives the mapping connection:

$$f_i = (m-1)T(r) = (m-1)\sum_{k=0}^{i}\frac{q_k}{Q} \quad (4)$$

where, q_k represents the number of pixels with the kth grey level, m specifies the number of grey levels contained in the original image, and Q represents the overall number of pixels in the image. If an image has n different grey levels and p_i represent the ith gray level occurrence probability, then the entropy of that level can be described as the following Eq. (5):

$$e(i) = -p_i log p_i \quad (5)$$

The entropy of the complete image is estimated using Eq. (6):

$$E = \sum_{i=0}^{n-1} e(i) = -\sum_{i=0}^{n-1} p_i \, log p_i \quad (6)$$

Eq. (6) shows that E will grow to its greatest value if $p_0 = p_{12} = \cdots p_{n-1} = \frac{1}{n}$. In other words, when the AHE of the image has a uniform distribution, the entropy of the entire image is at its highest. The findings of AHE are given in the gamma correction for further processing of the brain tumor image.

3.1.3 Gamma correction

The gamma correction procedure that can be utilized to control the overall brightness of the brain tumor image incorporates the AHE findings. It can be used on images that are overly contrasted or dark. Expanding and compressing pixel intensity levels is necessary for images that are fading and darker. Every pixel value undergoes gamma correction, a nonlinear adjustment. The majority of the time, subtraction, addition, and multiplication are applied to every pixel. The process of applying nonlinear algorithms to the input image's pixels and adjusting the image's saturation as a consequence is known as gamma correction. It is crucial to keep the gamma value constant because it shouldn't be too high or too low. The gamma correction parameter was selected based on its ability to adjust the enhance the image without overexposing or underexposing important features while it provided a good balance for the brain MRI images in our dataset.

3.2 Brain tumor segmentation using Aquila optimization-based K-means clustering

After preprocessing the brain tumor image, it undergoes segmentation to isolate the affected region in the brain. In this proposed model, an enhanced version of the K-means clustering algorithm is introduced, optimized using Aquila optimization. The segmentation strategy has been suggested to enhance unstable clustering and lessen its noise sensitivity. The Aquila optimization is applied to select the effective

cluster centroids in the image, which is done by maximum the PSNR value of the pixel present in the brain images. The process involved in the proposed segmentation algorithm is described as follows.

3.2.1 K-means clustering

The unsupervised learning model known as K-means is used to describe clustering. Models based on unsupervised learning are used for data sets that have never been labeled or categorized. Every data point is processed in line with these identical points, which are recorded in the data set. The model, which uses either a distance-based approach or a centroid-based technique, assigns points to each cluster in order to estimate the distance. After calculating a K value, divide the data into K categories to make it easier to distinguish between them. This will improve the data's similarity within each group. The distance is estimated using the Euclidean distance formula that is described below:

i) Euclidean Distance

Typically, Euclidean distance is used as an index to estimate the similarity among two sets of data. The Euclidean distance is the length of time in three dimensions between two places. The following equation gives a three-dimensional Eq. (7):

$$d = \sqrt{(x_1 - x_2)^2 + (y_1 - y_2)^2 + (z_1 - z_2)^3} \quad (7)$$

Additionally, it can be used for n-dimensional space, as given in the following Eq. (8):

$$d = \sqrt{\sum (x_{i1} - x_{i2})^2} \quad (8)$$

The ith dimensions coordinate of the first point is given as x_{i1}, and the ith dimensional coordinate of the second point is given as x_{i2}, where $i = 1,2,..,n$. Each point in the n-dimensional Euclidean space can be written as $,x(i) = (x(1), x(2),..x(n)$, where $i = 1,2,...n$ is a real number and is referred to as the ith coordinate of x. Eq. (8) is used to calculate the distance between two points x and y.

As the Euclidean distance between two sets of data decreases, so does the degree of similarity. Furthermore, each cluster is associated with one of the initial K centroids, and data points close to the centroid are classified as being a part of a cluster for classification purposes. To cluster the points as near to their respective cluster centroids as possible is the main goal of the iterative K-means algorithm. These perform three different processes. The first process is to choose K items to serve as the initial cluster's center in accordance with our study goal. Calculating the Euclidean distance between the data and the cluster center after classifying the data that are close together into one category. Recalculating the cluster centers of the recently split clusters is the second step, after which the clusters are divided once more using the initial divisions. The third process, the method can be terminated once this iterative process is completed and the cluster center no longer changes. The process can be stopped under three different conditions: first, the newly created cluster's centroid must remain intact; second, all of the points must remain in the same cluster; and third, it must complete the maximum number of iterations. Another indication that training should be expressly ended if, even after performing several iterations, these points are still in the same cluster. In this case, training should be terminated. When the allotted number of iterations has been reached, it can finally terminate the training.

3.2.2 Aquila optimization

Aquila optimization is a relatively new nature-inspired algorithm. The Aquila, a widely known species of bird of prey, is one of the most studied birds due to its hunting behavior. Males of the species are particularly efficient hunters, often capturing more prey when hunting alone. Aquilas rely on their speed and sharp talons to hunt animals such as rabbits, squirrels, and other creatures. They employ four distinct hunting techniques to capture their prey, demonstrating their ability to swiftly adapt their methods based on the situation. The four hunting techniques are described as follows.

- In the first method, the Aquila hunts by soaring at a great height before diving vertically towards its prey. After spotting its target, it executes a long, shallow glide, gradually increasing its speed as its wings fold. For this strategy to succeed, the Aquila must maintain a height advantage over its prey.
- In the second hunting method, the Aquila starts at a low altitude and relentlessly chases its target, whether it's flying or running. This approach is particularly effective for hunting seabirds, breeding grouse, or ground squirrels.
- The third hunting technique involves the Aquila flying at a low altitude, gradually descending as it approaches its prey. Once near the ground, the Aquila closes in on its target, aiming to land on the neck and back of the animal.
- The fourth technique, known as "walking and grabbing prey," sees the Aquila moving on the ground while using its beak to attract and seize its target.

The following is the mathematical expression of Aquila optimization. The Aquila method starts with N agents and a starting population of *X*, like other nature-inspired metaheuristic optimization algorithms in Eq. (9)

$$X_i(t+1) = X_b(t) \times \left(\frac{1-t}{T}\right) + (X_M(t) - X_b(t) * rand) \quad (9)$$

where, T signifies the total number of iterations, $(\frac{1-t}{T})$ is used to control the search process. The agent's exploration is updated based on the Levy flight distribution that is specified as $(Levy(D))$ and X_b in the second process. The following mathematical Eq. (10) defines this process:

$$X_i(t+1) = X_b(t) \times Levy(D) + X_R(t) + (y - x) * rand \quad (10)$$

The randomly selected agent is represented as X_R. Also, the spiral tracking shape are specified as x and y, which is mathematically formulated aa below:

$$X_i(t+1) = \left(X_b(t) - X_M(t)\right) \times \alpha - rand + ((UB - LB) \times rand + LB) \times \delta \quad (11)$$

The first process updates the agents based on X_M and X_b during the exploitation process and which is mathematically expressed as the following Eq. (11). During the exploitation process the adjustment parameters are considered as δ and α. Also, the randomly created parameters are specified as $rand \in [0,1]$. The agent is updated in the second strategy during the exploitation process according to the quality

functions such as, QF, X_b and Levy. The second process is mathematically expressed in the following Eq. (12):

$$X_i(t+1) = QF \times X_b(t) - (G_1 \times X(t) \times rand) - G_2 \times Levy(D) + rand \times G_1 \quad (12)$$

3.2.3 Selecting optimal cluster centroids through aquila optimization

By optimizing the PSNR value of the brain tumor imaging pixels, the ideal cluster centroids are chosen. PSNR is measured in decibels (dB). As the PSNR value increases, the quality of the reconstructed or compressed image improves. The MSE and PSNR are used to compare the quality of image compression. The most common application of the PSNR is to evaluate loss compression codes for recovered data. Here, the error caused by compression is the noise, while the original data is the signal.

$$PSNR = 10log_{10}\left(\frac{MAX_I^2}{MSE}\right) \quad (13)$$

$$MSE = \frac{1}{mn}\sum_{i=0}^{m-1}\sum_{j=0}^{n-1}[I(i,j) - K(i,j)]^2 \quad (14)$$

where, MAX_I^2 signified the maximum value of the pixel is in the original image, m represent the number of rows in the original image and n specifies the number of columns in the original image. With a size of $m \times n$, I and K denote original and contrast-enhanced images, respectively.

Step 1: *Initialization*

The pixels in the preprocessed images are considered for the problem in this research which is used to discover the optimal cluster centroid. The population is initialized using the following mathematical formula.

$$P = \{p_1, p_2, p_3, \ldots p_n\} \quad (15)$$

From Eq. (15), p_n specifies the number of pixels initialized in the population.

Step 2: *Fitness function*

The best centers for clustering in the brain tumor image are chosen using the fitness function. The maximum PSNR value of the pixel determines the ideal cluster center.

$$Fitness = \max\left(PSNR = 10log_{10}\left(\frac{MAX_I^2}{MSE}\right)\right) \quad (16)$$

Based on the above Eq. (16), the optimal cluster centroids are selected.

Step 3: *Updating*

To find the optimal cluster center within the pixels of the tumor image, the value of PSNR gets updated in each iteration.

Step 4: *Termination*

The optimal cluster centroid is discovered the process is ended.

3.2.4 Procedure of the proposed Aquila optimization-based K-means clustering

The following is the procedure that the suggested Aquila optimization-based K-means clustering (AOKC) algorithm uses.

Step 1: *Select the value for the number of clusters, k*

In this step, the specified number of clusters, denoted as k, are created.

Step 2: *Using AOKC, select k random points from the data to serve as centroids*

Then choosing the cluster centroids in the considered k number of clusters. The conventional K-means algorithm randomly selects the cluster centroids that is the major concern in the conventional algorithm. In order to address these concerns, the proposed model selects the optimal cluster centroid through Aquila optimization using Eq. (16).

Step 3: *Assign all the points to the closest cluster centroid*

Assign each point to the closest cluster centroid after the centroids have been initialized using the Aquila optimization method.

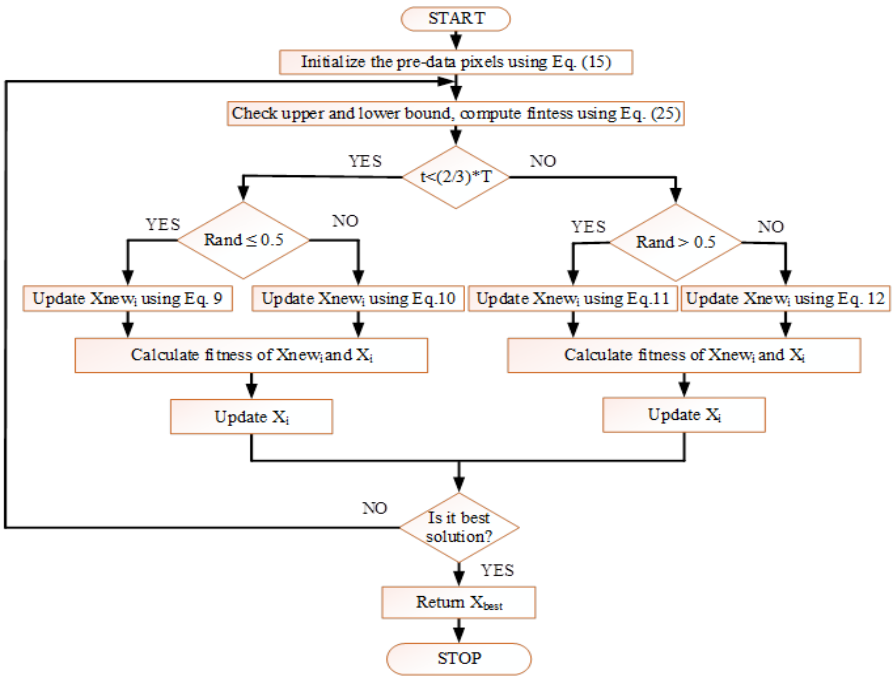

Figure 2. Flow chart of proposed Aquila optimization-based K-means clustering

Step 4: *Recomputed the centroids of newly formed clusters*

After all the points have been allocated to a cluster, the next step is to compute the centroids of newly formed clusters.

Step 5: *Repeat steps 3 and 4*

The process is repeated using steps 3 and 4. Figure 2 shows the overall process of selecting the pixel for K-means clustering.

One iteration is required to compute the centroid and allocate each point to the cluster based on far away it is from the centroid. Three criteria are used to terminate an improved K-means clustering process: The maximum number of iterations is reached, points remain in the same cluster, and the centroids of newly created clusters remain unchanged. According to the proposed segmentation algorithm the tumor tissues present in the brain images are effectively segmented which can used to the physicians for taking proper decision to save the patient's life. The segmented images are fed into CNN to validate the segmented image for diseases prediction. The pseudo code for the proposed algorithm is presented in Algorithm 1.

Algorithm 1: Pseudocode of the proposed AOCK algorithm

```
MRI brain image dataset = M
Begin
{
For all MRI images in the dataset
      # Pre-processing
            F = Median filter (M)                          //
noise removal of data
            N = Wiener filter (F)                          //
enhance quality of data
            E = Adaptive histogram equalization (N)        //
contrast enhancement of image
            G = Gamma Correction (E)                       //
improve pixel brightness
   # Segmentation
            S = AO- K means clustering (G)                 //
segment the brain tumor part
}
End
Output: segmented tumor tissue portion
```

4. RESULT AND DISCUSSION

This research proposes a K-means clustering technique for brain tumor segmentation based on Aquila optimization. The proposed segmentation algorithm is implemented using MATLAB to assess its performance, with the system featuring an Intel Core processor i5-330S CPU @ 2.70 GHz, a 64-bit operating system with an x64-based processor, and 8.00 GB of RAM. Table 1 shows the parameter for the proposed models: AOA and the CNN.

Table 1. Simulation parameter for the model

Simulation Parameter	Methods	Ranges
Dimensions	Aquila optimization algorithm (AOA)	2
Solution no		20
Maximum iterations		100
Alpha		0.1
Activation	Convolutional neural network (CNN)	Softmax
optimizer		Adam
Learning rate		0.001

***Dataset Description*:** The dataset consists of 7,022 labeled brain MRI images categorized into four classes such as glioma, meningioma, no tumor, and pituitary tumor. It includes 1,311 images designated for testing, with 300 images each for glioma, meningioma, and pituitary tumor classes, and 405 images for the no tumor class. These images vary in size, and preprocessing (including resizing) [21]. The training values are taken in 5711, while the testing data is 1311.

From the Table 2, the first column illustrates the sample input brain images. Then, the second column is the findings of denoised images which is performed using median and wiener filters. The findings of the denoising phase are provided as the input of the AHE and the output of AHE is given in the third column of the above table. Finally, in the preprocessing stage performed gamma correction for controlling the entire brightness of the brain MRI which is provided in the final column. After preprocessing, the brain images which is considered as the input of the segmenting process.

Table 3 compares the segmentation results of the known techniques, such as FCM and K-means clustering, with the proposed AOKC. Table 2's first column presents the segmentation results of the suggested AOKC algorithm. The results of the FCM and K-means algorithms are displayed in the column that follows. When comparing the proposed segmented image with existing segmented images, the proposed segmented image properly segments the tumor portions in the brain.

Table 4 displays the comparison of segmented images using the proposed algorithm and ground truth images. The segmented image through the proposed AOKC algorithm displays the first column and the second column specifies the ground truth brain MRI. When analyzing these two segmented portions almost two segmented portions are equal and this demonstrates the efficacy of the suggested segmentation algorithm.

Table 2. Preprocessed findings of the sample brain magnetic resonance imaging (MRI)

Input Image	Image Denoising		Adaptive Histogram Equalization	Gamma Correction
	Median Filter	Weiner Filter		
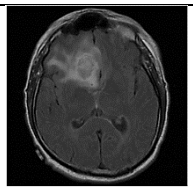	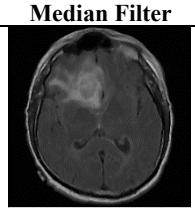	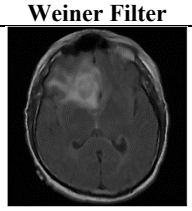	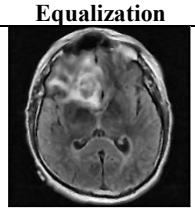	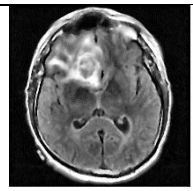

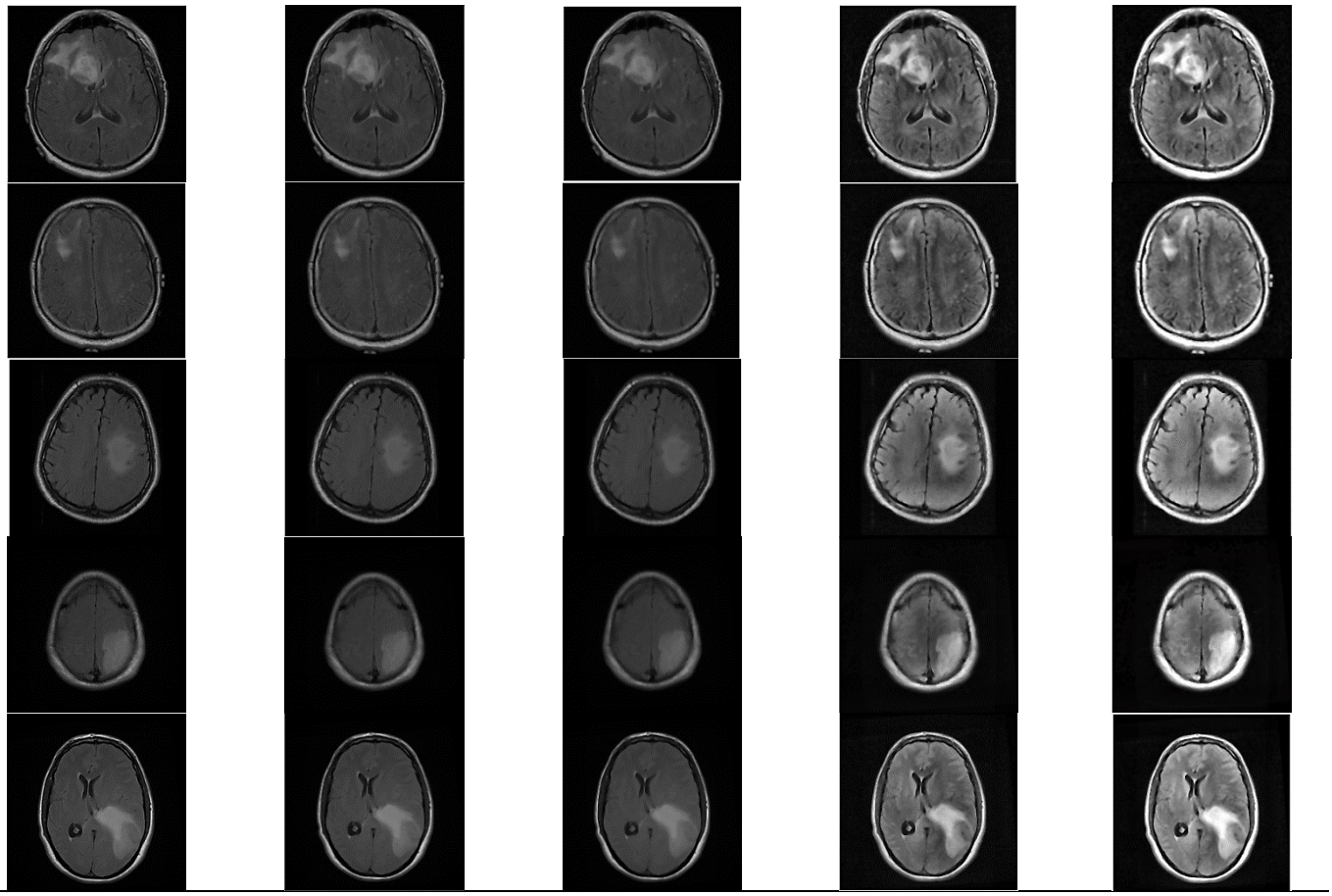

Table 3. Comparison of segmentation findings among proposed and existing

Proposed Aquila Optimization Based K-Means Clustering	K-Means Clustering	Fuzzy C Means
		
	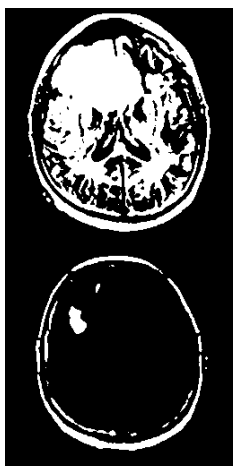	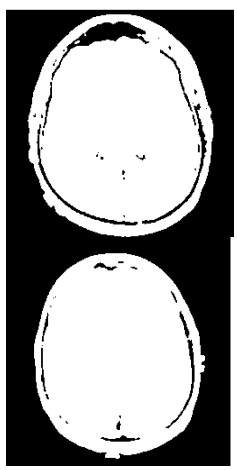

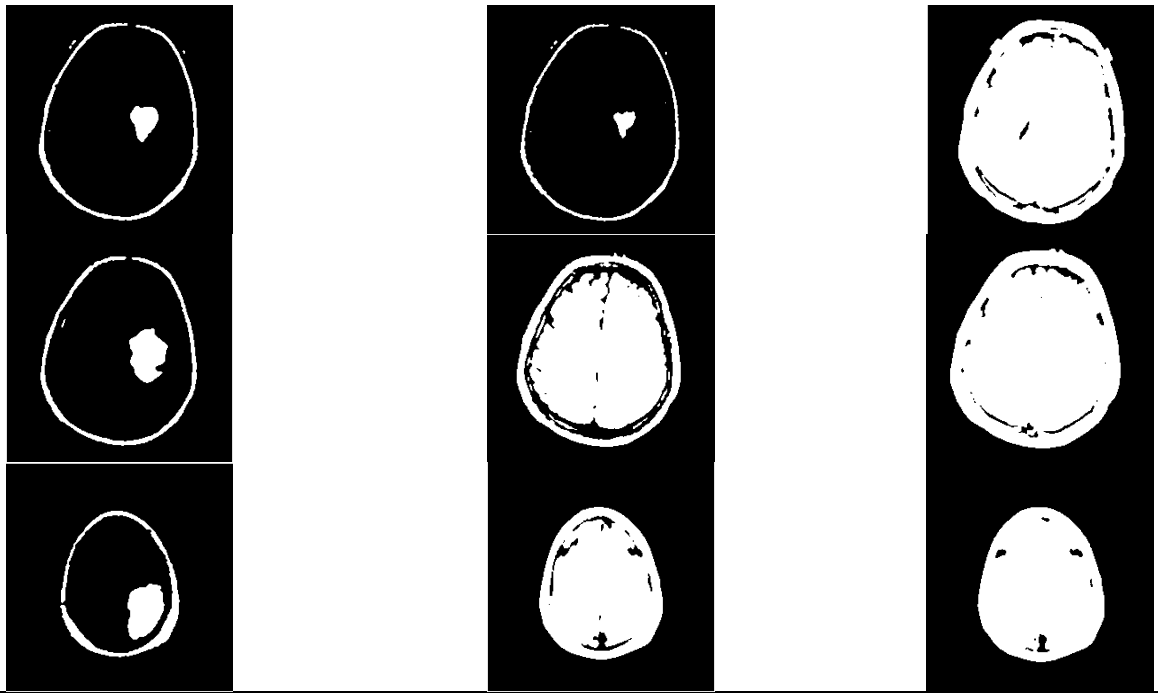

Table 4. Comparison of segmented images using proposed algorithm and ground truth images

Ground Truth Brain Magnetic Resonance Imaging	Segmented Image Through Proposed Aquila Optimization Based K-Means Clustering

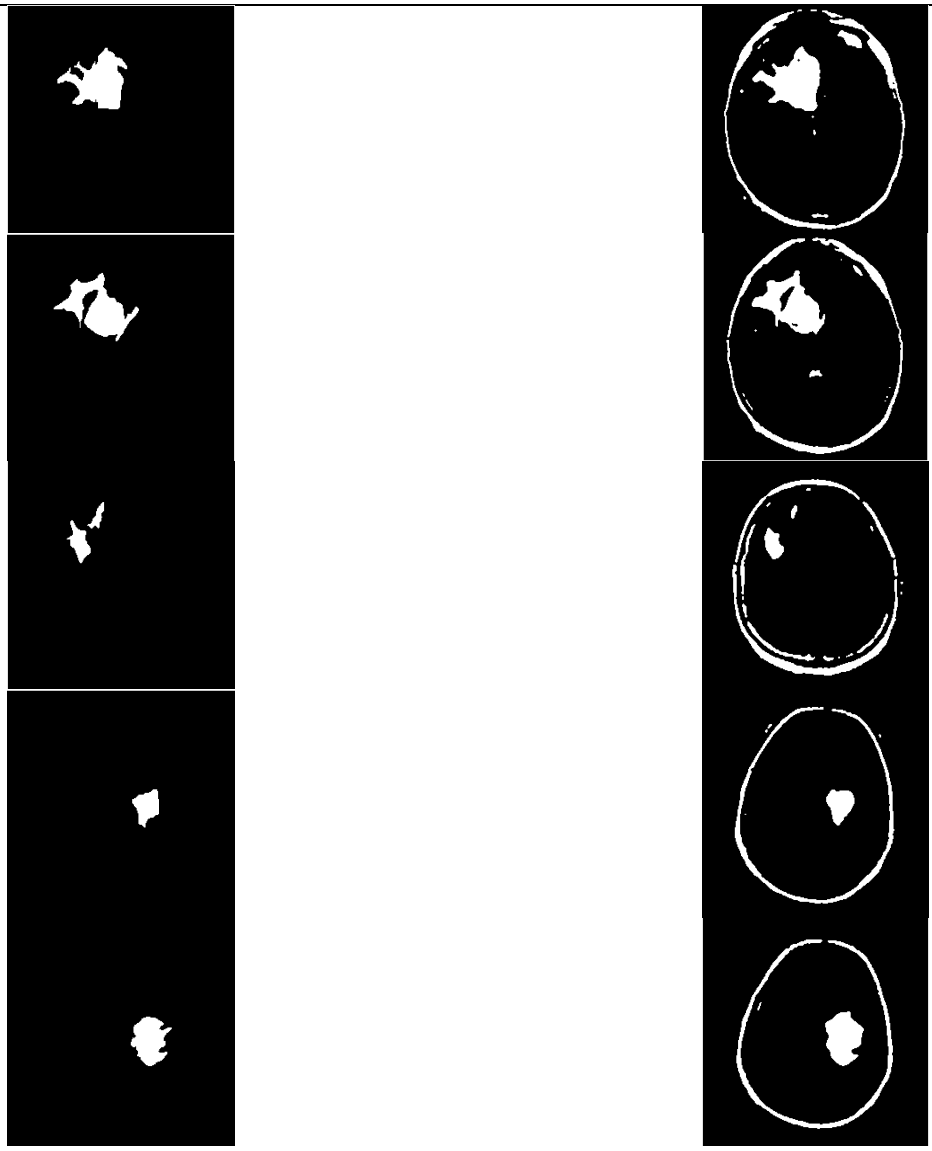

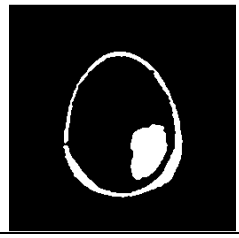

4.1 Performance analysis

The confusion matrix demonstrates the classification performance of the model in Figure 3. Validate the performance improvements of the CNN model for brain tumor classification. The model performs well, with the highest number of correct predictions for No Tumor (398), followed by Meningioma (299), Pituitary (295), and Glioma (292). However, there are some misclassifications, particularly between similar tumor types such as Glioma and Meningioma, and between No Tumor and Pituitary. For example, a few Gliomas were predicted as Meningiomas, and some Pituitary cases were misclassified as No Tumor.

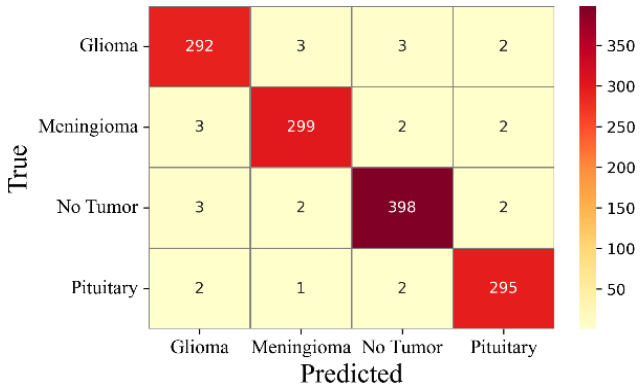

Figure 3. Confusion matrix for the proposed model

In this segment, the proposed wiener filter performance metrics are compared to some other traditional techniques like Gaussian filter, mean filter, and bilateral filter. The Gaussian Filter (GF), Mean Filter (MF), and Bilateral Filter (BF) are contrasted with the Wiener Filter (WF) images. The following figure presents a comparison of pre-data indicators.

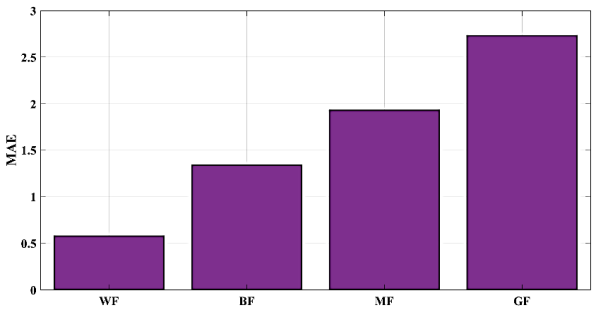

Figure 4. Comparison of mean absolute error

The approach depicted in Figure 4 is validated by examining the mean absolute error (MAE) and contrast the observed values with the convolution model. The proposed WF model's MAE is 0.0605, BF offers 1.35, MF offers 1.95, and GF offer 2.7 MAE. Therefore, it shows that the suggested model has a lower error value than the traditional approaches. Figure 5 demonstrates the root mean square error (RMSE) comparison. It shows the proposed WF provides 2.5 RMSE, BF provides 5.4 RMSE, MF provides 5.2 RMSE and GF offers 6.4 RMSE. It shows the WF have low RMSE value than the traditional models. Further feature similarity index method (FSIM) is analyzed and illustrated in Figure 6. It shows the proposed WF provides 0.98 FSIM, BF provides 0.85 FSIM, MF provides 82 FSIM and GF offers 72 FSIM. It shows the WF have high FSIM value than the traditional models.

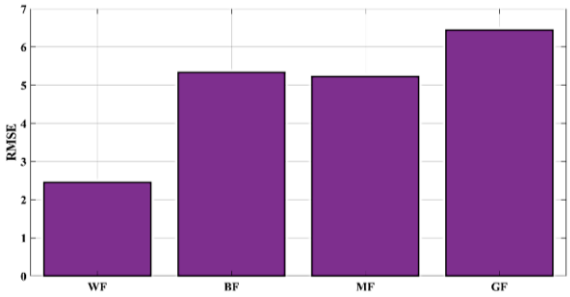

Figure 5. Comparison of root mean square error

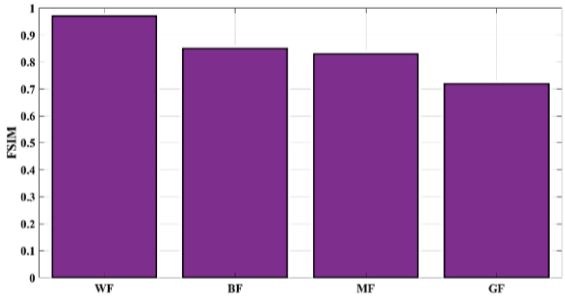

Figure 6. Comparison of feature similarity index method

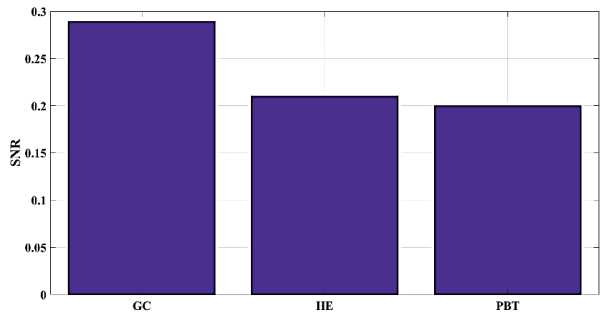

Figure 7. Comparison of Signal-to-Noise Ratio

The Signal-to-Noise Ratio (SNR) of the suggested gamma correction (GC) model is compared with traditional models like histogram equalization (HE), Pixel brightness transformations (PBT). In Figure 7, the suggested GC model has 0.29 SNR, HE has 0.21 SNR, and PBT has 0.2 SNR. This indicates that compared to other models, the recommended model delivers a greater SNR value. Figure 8 shows the mean

luminous of GC images with its comparison was provided. The mean luminous of GC is 80, HE is 73, and PBT is 69. It verifies that the proposed model provides a better outcome than traditional models. The methods described in Figure 9 can be tested by comparing the PSNR of the suggested model. The suggested GC model provides 42 PSNR, HE provides 35 PSNR, and PBT provides 29.5 PSNR. The outcome demonstrates that the proposed offers better value than the traditional models.

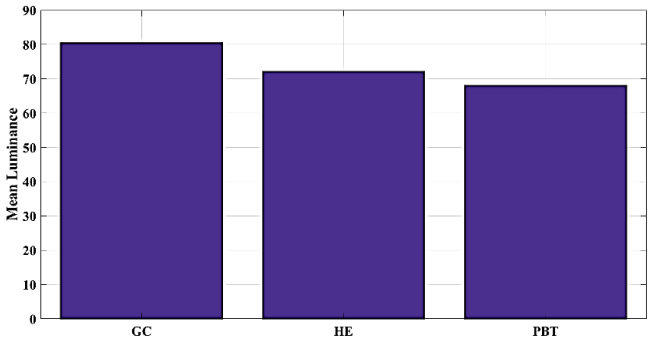

Figure 8. Comparison of mean luminance

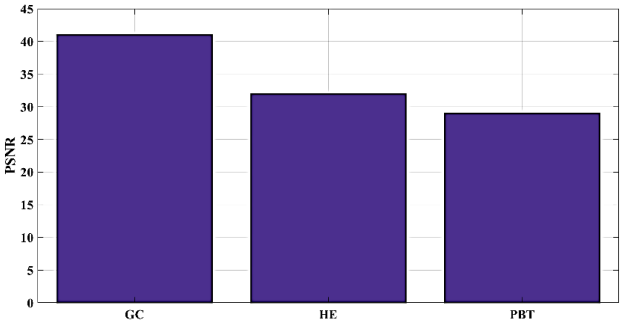

Figure 9. Comparison of Peak Signal-to-Noise Ratio

The proposed segmentation algorithm's experimental analysis is tested with several performance metrics like, Bit Error Rate (BER), PSNR, MSE, Structural Similarity Index Measure (SSIM), and Normalized Correlation (NC). Moreover, the performance is analyzed by comparing several existing segmentation algorithms like, K-means clustering and FCM.

Comparison of PSNR is displayed in Figure 10. Here, the comparison is done among the proposed AOKC and existing algorithms. In addition, there are five different samples are considered for this analysis that is named as sample 1, 2, 3, 4 and sample 5. For sample 1, the PSNR value of the proposed model attained 59.95 (dB), the K-means and FCM attained PSNR of 51.11 (dB) and 50.80 (dB). For sample 2, the PSNR value of the proposed model attained 60.14 (dB), the K-means and FCM attained PSNR of 51.26 (dB) and 50.91 (dB). For sample 3, the PSNR value of the proposed model attained 59.85 (dB), the K-means and FCM attained PSNR of 51.37 (dB) and 51.14 (dB). For sample 4, the PSNR value of the proposed model attained 61.70(dB), the K-means and FCM attained PSNR of 52.17 (dB) and 51.46 (dB). For sample 5, the PSNR value of the proposed model attained 61.20 (dB), the K-means and FCM attained PSNR of 52.36 (dB) and 51.74 (dB). When compared to the existing method the proposed AOKC algorithm attained maximum PSNR value.

Comparison of BER is displayed in Figure 11. Here, the comparison is done among the proposed AOKC and existing algorithms. In addition, there are five different samples are considered for this analysis that is named as, sample 1, sample 2, sample 3, sample 4 and sample 5. For sample 1, BER value of the proposed model attained 0.0166, the K-means and FCM attained BER of 0.0195 and 0.0196. For sample 2, the BER value of the proposed model attained 0.01662, the K-means and FCM attained BER of 0.0195 and 0.1964. For sample 3, the BER value of the proposed model attained 0.0165, the K-means and FCM attained BER of 0.0167 and 0.0195. For sample 4, the BER value of the proposed model attained 0.0162, the K-means and FCM attained BER of 0.0191 and 0.0194. For sample 5, the BER value of the proposed model attained 0.0163, the K-means and FCM attained BER of 0.0190 and 0.0193. When compared to the existing method the proposed AOKC algorithm attained less BER value.

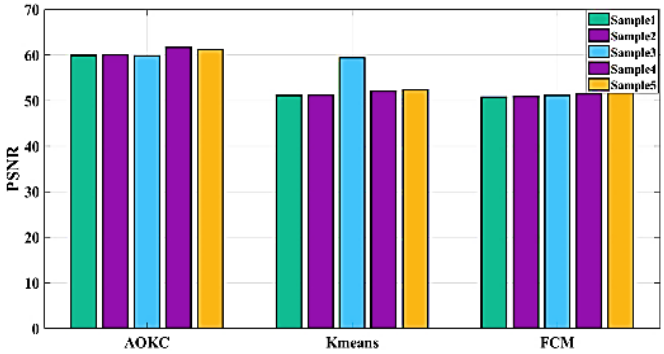

Figure 10. Comparison of Peak Signal-to-Noise Ratio

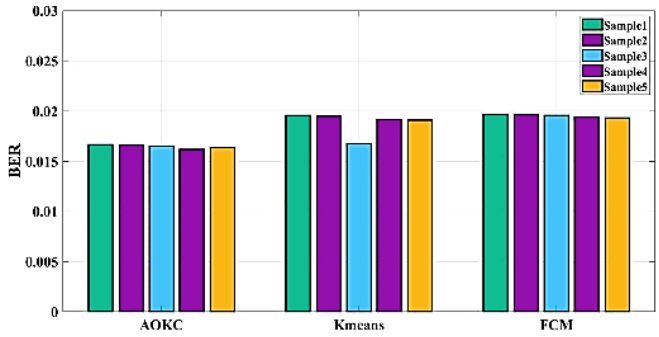

Figure 11. Comparison of Bit Error Rate

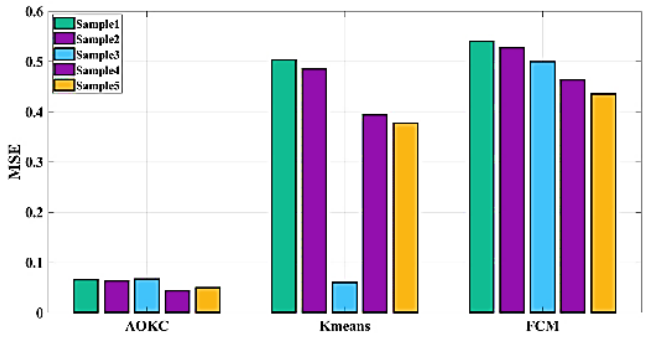

Figure 12. Comparison of mean square error

Comparison of MSE is displayed in Figure 12. Here, the comparison is done among the proposed AOKC and existing algorithms. In addition, there are five different samples are considered for this analysis that is named as, samples 1, 2, 3, 4 and 5. For sample 1, the MSE value of the proposed model attained 0.0656, the K-means and FCM attained MSE of

0.5034 and 0.5406. For sample 2, the MSE value of the proposed model attained 0.0629, the K-means and FCM attained MSE of 0.4854 and 0.5272. For sample 3, the MSE value of the proposed model attained 0.0673, the K-means and FCM attained MSE of 0.0597 and 0.4996. For sample 4, the MSE value of the proposed model attained 0.0439, the K-means and FCM attained MSE of 0.3941 and 0.4640. For sample 5, the MSE value of the proposed model attained 0.0493, the K-means and FCM attained MSE of 0.3774 and 0.4349. The proposed AOKC algorithm achieved a lower MSE value in comparison to the current technique.

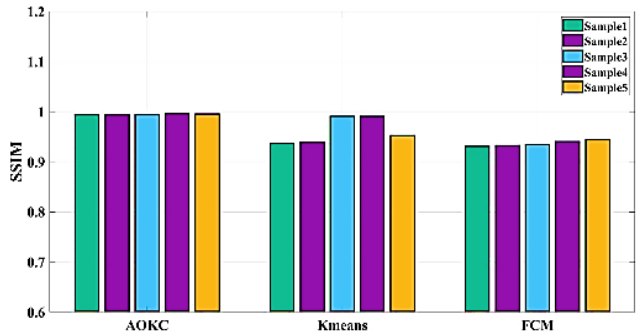

Figure 13. Comparison of Structural Similarity Index Measure

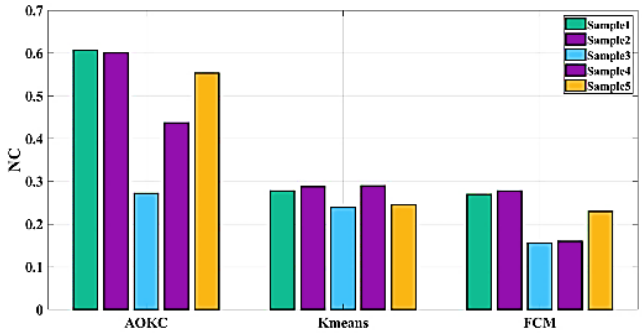

Figure 14. Comparison of Normalized Correlation

Comparison of SSIM is displayed in Figure 13. Here, the comparison is done among the proposed AOKC and existing algorithms. In addition, there are five different samples are considered for this analysis that is named as, samples 1, 2, 3, 4 and 5. For sample 1, the SSIM value of the proposed model attained 0.9937, the K-means and FCM attained SSIM of 0.9366 and 0.9309. For sample 2, the SSIM value of the proposed model attained 0.9940, the K-means and FCM attained SSIM of 0.9392 and 0.9329. For sample 3, the SSIM value of the proposed model attained 0.9936, the K-means and FCM attained SSIM of 51.37 and 51.14. For sample 4, the SSIM value of the proposed model attained 61.70, the K-means and FCM attained SSIM of 0.9905 and 0.9353. For sample 5, the SSIM value of the proposed model attained 0.9953, the K-means and FCM attained SSIM of 0.9527 and 0.9438. When compared to the existing method the proposed AOKC algorithm attained maximum SSIM value.

Comparison of NC is displayed in Figure 14. Here, the comparison is done among the proposed AOKC and existing algorithms. In addition, there are five different samples are considered for this analysis that is named as, samples 1, 2, 3, 4 and 5. For sample 1, the NC value of the proposed model attained 0.6065, the K-means and FCM attained NC of 0.2780 and 26.90. For sample 2, the NC value of the proposed model attained 0.6010, the K-means and FCM attained NC of 0.2879 and 0.2772. For sample 3, the NC value of the proposed model attained 0.2721, the K-means and FCM attained NC of 0.2383 and 0.1554. For sample 4, the NC value of the proposed model attained 0.4368, the K-means and FCM attained SSIM of 0.2900 and 0.1602. For sample 5, the NC value of the proposed model attained 0.5527, the K-means and FCM attained NC of 0.2451 and 0.2293. When compared to the existing method the proposed AOKC algorithm attained maximum NC value.

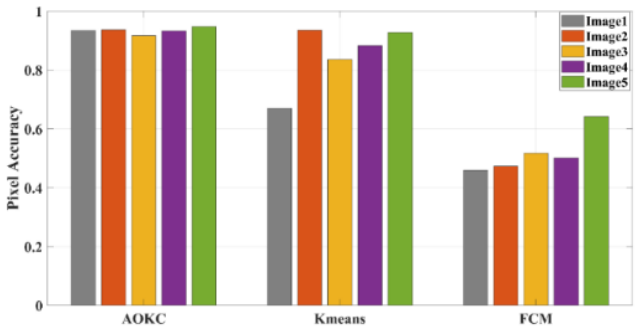

Figure 15. Comparison of pixel accuracy

Comparison of pixel accuracy is illustrated in Figure 15. For sample 1, the pixel accuracy value of the proposed model attained 0.934, the K-means and FCM achieved 0.670 and 0.459, respectively. For sample 2, the pixel accuracy value of the proposed model attained 0.937, the K-means and FCM achieved 0.935 and 0.472 respectively. For sample 3, the pixel accuracy value of the proposed model attained 0.917, the K-means and FCM achieved 0.835 and 0.517. For sample 4, the pixel accuracy value of the proposed model achieved 0.932, the K-means and FCM attained 0.883 and 0.500 respectively. For sample 5, the pixel accuracy value of the proposed model achieved 0.947, the K-means and FCM achieved 0.927 and 0.641 respectively. When compared to the existing method the proposed AOKC algorithm attained maximum pixel accuracy value.

Figure 16 compares the Jaccard index of proposed and current approaches. For sample 1, the proposed model's Jaccard index value was 0.701, while the FCM and K-means values were 0.480 and 0.112, respectively. The suggested model's Jaccard index value for sample 2 was 0.714, while the FCM and K-means achieved 0.717 and 0.119, respectively. In sample 3, the suggested model's Jaccard index value was 0.694, while the K-means and FCM values were 0.617 and 0.319, respectively. The proposed model's Jaccard index value for sample 4 was 0.669, while the K-means and FCM values were 0.310 and 0.036, respectively. The proposed model's Jaccard index value for sample 5 was 0.736, whereas the FCM and K-means achieved 0.714 and 0.145, respectively. In contrast to the current approach, the proposed AOKC algorithm attained the maximum Jaccard index value.

A comparison of the dice coefficient is illustrated in Figure 17. For sample 1, the dice coefficient value of the proposed model attained 0.824, the K-means and FCM achieved 0.305 and 0.202 respectively. For sample 2, the dice coefficient value of the proposed model attained 0.833, the K-means and FCM achieved 0.835 and 0.214 respectively. For sample 3, the dice coefficient value of the proposed model attained 0.853, the K-means and FCM achieved 0.623 and 0.261. For sample 4, the dice coefficient value of the proposed model attained

0.790, the K-means and FCM achieved 0.599 and 0.207 respectively. For sample 5, the dice coefficient value of the proposed model attained 0.847, the K-means and FCM achieved 0.846 and 0.254 respectively. Compared to the existing method, the proposed AOKC algorithm achieved a higher dice coefficient value.

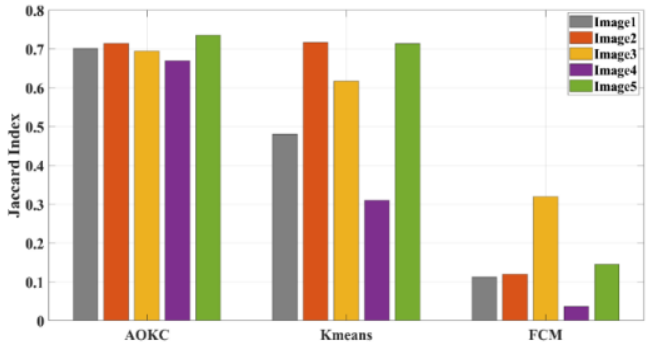

Figure 16. Comparison of Jaccard index

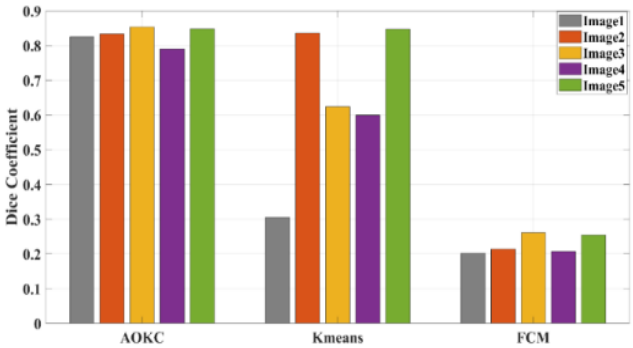

Figure 17. Comparison of dice coefficient

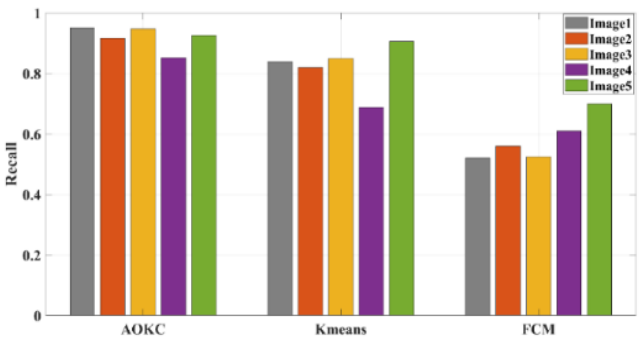

Figure 18. Comparison of recall

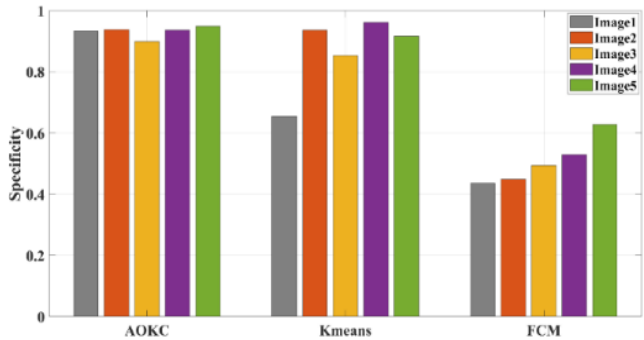

Figure 19. Comparison of specificity

Figure 18 compares the recall of proposed and current approaches. For sample 1, the proposed model's recall value was 0.951, while the FCM and K-means values were 0.84 and 0.52, respectively. The suggested model's recall value for sample 2 was 0.917, while the FCM and K-means achieved 0.819 and 0.56, respectively. In sample 3, the suggested model's recall value was 0.947, while the K-means and FCM values were 0.849 and 0.525, respectively. The proposed model's recall value for sample 4 was 0.852, while the K-means and FCM values were 0.688 and 0.61, respectively. The proposed model's recall value for sample 5 was 0.926, whereas the FCM and K-means achieved 0.905 and 0.7, respectively. In contrast to the current approach, the proposed AOKC algorithm attained better recall value.

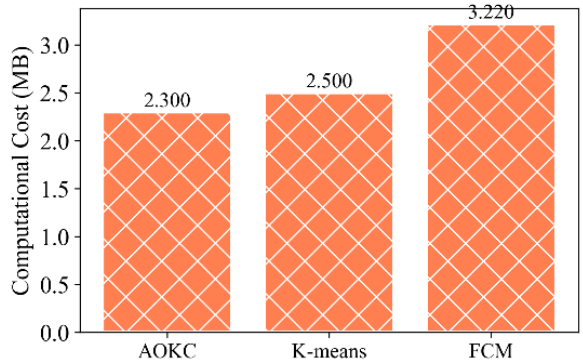

Figure 20. Analysis of computational cost

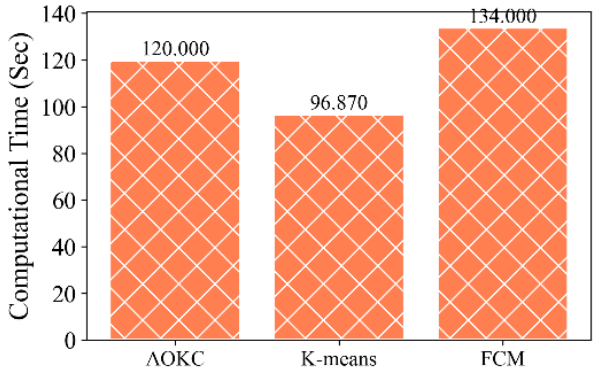

Figure 21. Evaluation of the proposed and existing model in computational time

A comparison of specificity is illustrated in Figure 19. For sample 1, the specificity value of the proposed model attained 0.933, the K-means and FCM achieved 0.655 and 0.435 respectively. For sample 2, the specificity value of the proposed model achieved 0.938, the K-means and FCM achieved 0.936 and 0.448 respectively. For sample 3, the specificity value of the proposed model achieved 0.898, the K-means and FCM achieved 0.853 and 0.494. For sample 4, the specificity value of the proposed model achieved 0.936, the K-means and FCM achieved 0.961 and 0.529 respectively. For sample 5, the specificity value of the proposed model achieved 0.948, the K-means and FCM achieved 0.916 and 0.628 respectively. Compared to the existing method, the proposed AOKC algorithm offers a high specificity value.

Figures 20 and 21 present an evaluation of the computational cost and time for three models. The proposed model is 2.3 MB while the existing model 2.5 MB, 3.2 MB. Regarding computational time (Figure 20). AOKC at 120 seconds the various model in K-means and FCM at 96.87 sec,

134 sec.

Table 5 presents statistical tests of the proposed model. The tests include McNemar, Friedman, Wilcoxon, paired t-test, and Analysis of Variance, all of which yield p-values less than 0.05, indicating statistically significant differences in performance.

Table 6 presents the cross-validation results for the proposed model. The performance across five folds with metrics such as MSE, dice coefficient, PSNR, and Jaccard Index. The model demonstrates consistent and strong performance, with fold 4 achieving the best results in all metrics. The lowest MSE (0.065), highest dice coefficient (0.824), highest PSNR (60.14 dB), and highest Jaccard Index (0.701). These results indicate that the proposed model provides optimal segmentation accuracy, image quality, and minimal prediction error, with fold 4 showcasing its best overall performance.

Table 5. Statistical test for the proposed model

Test	Value	P Value
McNemar	$X^2 = 1$	0.044
Friedman	$X^2 = 8.12$	0.017
Wilcoxon	$W = 15$	0.042
Paired t-test	$t = 2.06$	0.044
Analysis of Variance	$F = 4.18$	0.018

Table 6. Cross validation for the suggested model

Fold	Mean-Square Error (dB)	Dice Coefficient	Peak Signal-to-Noise Ratio	Jaccard Index
1	0.085	0.75	45.2	0.601
2	0.095	0.65	55.8	0.62
3	0.075	0.78	58.4	0.59
4	**0.065**	**0.824**	**60.14**	**0.701**
5	0.096	0.55	44.2	0.69

Table 7. State of art for the proposed segmentation method

Model	Mean Square Error	Dice Coefficient	Peak Signal-to-Noise Ratio	Processing Time (sec)
Aquila Optimization-based K-means Clustering (proposed)	0.065	0.824	60.14	120
Elephant Herding Optimization Algorithm with Entropy-Driven Fuzzy C-Means [16]	0.29	0.80	53.57	26.57
K-means Clustering [19]	-	0.78	-	-
Fuzzy C-Means [22]	-	0.96	-	-
Greedy Snake Model and Fuzzy C Means Optimization [23]	-	0.79	-	-

Table 7 shows the various state of art model. AOKC is developed as an improved brain tumor segmentation model. The AOKC model, proposed in this study, demonstrates the best overall performance, with a low MSE of 0.065, a high Dice Coefficient of 0.824, and an excellent PSNR of 60.14 dB, while taking 120 seconds for processing. This balance of accuracy and reasonable processing time makes it highly suitable for clinical applications. In comparison, the EHO with EnFCM model, though faster (26.57 seconds), has a higher MSE (0.29) and lower dice coefficient (0.80), indicating less accurate segmentation. The K-means clustering model, while simple, shows moderate performance with a dice coefficient of 0.78 but lacks MSE and PSNR values. AOKC offers greater stability by utilizing an optimization algorithm (Aquila) to select centroids from the tumor dataset, thus eliminating the need for fine-tuning of parameters and giving AOKC greater generalizability to other tumor datasets than previous models.

The proposed AOKC algorithm demonstrates significant improvements in brain tumor segmentation compared to traditional methods like K-means and FCM, achieving higher accuracy in key performance metrics such as PSNR, SSIM, BER, recall, and dice coefficient. The use of Aquila optimization to enhance centroid selection in K-means clustering improves the algorithm's ability to distinguish tumor regions from healthy tissue, resulting in better segmentation quality. Preprocessing steps like Wiener filtering, AHE, and gamma correction further contribute to higher image quality, enhancing the effectiveness of segmentation. The AOKC algorithm also excels in specificity, ensuring accurate identification of non-tumor regions, which was crucial in clinical applications. Although the algorithm's computational time was slightly longer than existing methods, its superior performance in tumor detection justifies the added time, making it a viable tool for medical imaging.

5. CONCLUSION

This research presents a K-means clustering algorithm for efficient brain tumor segmentation, optimized using Aquila optimization. Brain tumor segmentation is the process of automatically classifying malignant brain tissues according to the types of tumors by identifying them. Tumor segmentation from brain MRIs by hand is labor-intensive and prone to mistakes. A quick and precise method for segmenting brain tumors is required. Based on this need, in the proposed model, an optimal clustering segmentation was developed to detect the tumor in an MRI image. The initial phase is image preprocessing, which is performed to enrich the image quality as well as image features for attaining accurate findings. Image denoising, AHE and gamma correction are applied in the preprocessing phase. An AHE is used after noise reduction to improve the contrast of the images of brain tumors. At last, a gamma correction was applied during the preprocessing stage to regulate the brain tumor image's overall brightness. After preprocessing, the segmentation step receives the pre-data image as input. Here, segmentation is carried out effectively with the use of enhanced k-means clustering. It is a well-liked option for clustering tasks since it is simple to comprehend and apply, computationally efficient, and capable of handling big datasets with high dimensionality. By selecting the ideal cluster centroids with efficiency, the Aquila optimization method enhances the performance of k-means clustering. Because Aquila optimization have a strong capacity for worldwide detection, excellent search efficacy, and quick convergence. This overcomes the limitations of the traditional

k-means clustering method, enabling more efficient segmentation. The proposed segmentation algorithm is implemented on MATLAB software to estimate its effectiveness. Several prior algorithms like k-means and FCM are taken for this analysis. BER, PSNR, SSIM, MSE and NC are the considered performance metrics used in this analysis. The AOKC attained PSNR of 60.14 (dB), BER have 0.016, MSE have 0.065, SSIM have 0.99 and 0.60 of NC, while compared to the other algorithm the proposed AOKC algorithm achieved better results. This reveals the effectiveness of the proposed AOKC algorithm which can be useful for segmenting the tumor images. In future work, segmentation of brain tumor will be done through a neural network or advanced approach-based segment process. Additionally, the application of Aquila optimization could be extended or replaced with other hybrid optimization techniques or deep learning approaches to further improve segmentation accuracy, especially in multi-modal or 3D imaging scenarios. Additionally, the real-world applications, including real-time hospital deployment for tumor detection, 3D segmentation for volumetric tumor analysis, and multi-modal imaging integration to enhance segmentation accuracy across different imaging modalities.

REFERENCE

[1] Ali, M., Gilani, S.O., Waris, A., Zafar, K., Jamil, M. (2020). Brain tumour image segmentation using deep networks. IEEE Access, 8: 153589-153598. https://doi.org/10.1109/ACCESS.2020.3018160

[2] Karayegen, G., Aksahin, M.F. (2021). Brain tumor prediction on MR images with semantic segmentation by using deep learning network and 3D imaging of tumor region. Biomedical Signal Processing and Control, 66: 102458. https://doi.org/10.1016/j.bspc.2021.102458

[3] Naser, M.A., Deen, M.J. (2020). Brain tumor segmentation and grading of lower-grade glioma using deep learning in MRI images. Computers in Biology and Medicine, 121: 103758. https://doi.org/10.1016/j.compbiomed.2020.103758

[4] Ramesh, S., Sasikala, S., Paramanandham, N. (2021). Segmentation and classification of brain tumors using modified median noise filter and deep learning approaches. Multimedia Tools and Applications, 80: 11789-11813. https://doi.org/10.1007/s11042-020-10351-4

[5] Kshirsagar, P.R., Rakhonde, A.N., Chippalkatti, P. (2020). MRI image based brain tumor detection using machine learning. Test Engineering and Management, 81: 3672-3680.

[6] Vijh, S., Sharma, S., Gaurav, P. (2020). Brain tumor segmentation using OTSU embedded adaptive particle swarm optimization method and convolutional neural network. Data Visualization and Knowledge Engineering: Spotting Data Points with Artificial Intelligence, 171-194. https://doi.org/10.1007/978-3-030-25797-2_8

[7] Noreen, N., Palaniappan, S., Qayyum, A., Ahmad, I., Imran, M., Shoaib, M. (2020). A deep learning model based on concatenation approach for the diagnosis of brain tumor. IEEE Access, 8: 55135-55144. https://doi.org/10.1109/ACCESS.2020.2978629

[8] Şişik, F., Eser, S.E.R.T. (2020). Brain tumor segmentation approach based on the extreme learning machine and significantly fast and robust fuzzy C-means clustering algorithms running on Raspberry Pi hardware. Medical Hypotheses, 136: 109507. https://doi.org/10.1016/j.mehy.2019.109507

[9] Li, H., Li, A., Wang, M. (2019). A novel end-to-end brain tumor segmentation method using improved fully convolutional networks. Computers in Biology and Medicine, 108: 150-160. https://doi.org/10.1016/j.compbiomed.2019.03.014

[10] Alqazzaz, S., Sun, X., Yang, X., Nokes, L. (2019). Automated brain tumor segmentation on multi-modal MR image using SegNet. Computational Visual Media, 5(2): 209-219. https://doi.org/10.1007/s41095-019-0139-y

[11] Pitchai, R., Supraja, P., Victoria, A.H., Madhavi, M. J.N.P.L. (2021). Brain tumor segmentation using deep learning and fuzzy K-means clustering for magnetic resonance images. Neural Processing Letters, 53: 2519-2532. https://doi.org/10.1007/s11063-020-10326-4

[12] Karthick, S., Muthukumaran, N. (2024). Deep RegNet-150 architecture for single image super resolution of real-time unpaired image data. Applied Soft Computing, 162: 111837. https://doi.org/10.1016/j.asoc.2024.111837

[13] Sajja, V.R., Kalluri, H.K. (2020). Brain tumor segmentation using fuzzy C-means and tumor grade classification using SVM. In Smart Technologies in Data Science and Communication: Proceedings of SMART-DSC 2019, pp. 197-204. https://doi.org/10.1007/978-981-15-2407-3_24

[14] Sheela, C.J.J., Suganthi, G. (2022). Automatic brain tumor segmentation from MRI using greedy snake model and fuzzy C-means optimization. Journal of King Saud University-Computer and Information Sciences, 34(3): 557-566. https://doi.org/10.1016/j.jksuci.2019.04.006

[15] Thaha, M.M., Kumar, K.P.M., Murugan, B.S., Dhanasekeran, S., Vijayakarthick, P., Selvi, A.S. (2019). Brain tumor segmentation using convolutional neural networks in MRI images. Journal of Medical Systems, 43: 294. https://doi.org/10.1007/s10916-019-1416-0

[16] Karun, B., Thiyagarajan, A., Murugan, P.R., Jeyaprakash, N., Ramaraj, K., Makreri, R. (2024). Advanced hybrid brain tumor segmentation in MRI: elephant herding optimization combined with entropy-guided fuzzy clustering. Mathematical and Computational Applications, 30(1): 1. https://doi.org/10.3390/mca30010001

[17] Islam, M.K., Ali, M.S., Miah, M.S., Rahman, M.M., Alam, M.S., Hossain, M.A. (2021). Brain tumor detection in MR image using superpixels, principal component analysis and template based K-means clustering algorithm. Machine Learning with Applications, 5: 100044. https://doi.org/10.1016/j.mlwa.2021.100044

[18] Sharif, M., Tanvir, U., Munir, E.U., Khan, M.A., Yasmin, M. (2024). Brain tumor segmentation and classification by improved binomial thresholding and multi-features selection. Journal of Ambient Intelligence and Humanized Computing, 15(1): 1063-1082. https://doi.org/10.1007/s12652-018-1075-x

[19] Sahoo, A.K., Parida, P., Muralibabu, K. (2024). Hybrid deep neural network with clustering algorithms for effective gliomas segmentation. International Journal of System Assurance Engineering and Management, 15(3):

964-980. https://doi.org/10.1007/s13198-023-02183-w
[20] Kumar, D.M., Satyanarayana, D., Prasad, M.G. (2021). MRI brain tumor detection using optimal possibilistic fuzzy C-means clustering algorithm and adaptive k-nearest neighbor classifier. Journal of Ambient Intelligence and Humanized Computing, 12(2): 2867-2880. https://doi.org/10.1007/s12652-020-02444-7
[21] Brain Tumor MRI Dataset. https://www.kaggle.com/datasets/masoudnickparvar/brain-tumor-mri-dataset.
[22] Alqhtani, S.M., Soomro, T.A., Shah, A.A., Memon, A.A., et al. (2024). Improved brain tumor segmentation and classification in brain MRI with FCM-SVM: A diagnostic approach. IEEE Access, 12: 61312-61335. https://doi.org/10.1109/ACCESS.2024.3394541
[23] Sheela, C.J.J., Suganthi, G. (2022). Automatic brain tumor segmentation from MRI using greedy snake model and fuzzy C-means optimization. Journal of King Saud University-Computer and Information Sciences, 34(3): 557-566. https://doi.org/10.1016/j.jksuci.2019.04.006